

AN EXPERIMENTAL INVESTIGATION OF DEBRIS CLOUD GENERATED BY HYPERVELOCITY IMPACT OF ALUMINUM SPHERES WITH ALUMINUM SHEETS

R.Q. Chi, B.J. Pang, G.S. Guan, Z.Q. Yang, L.W. Wang

Hypervelocity Impact Research Center, Harbin Institute of Technology, P. O. Box 3020, No.2 Yikuang Street, Nangang District, Harbin 150080, P.R. China, Email: chirg@hit.edu.cn

ABSTRACT

Debris clouds generated in hypervelocity tests using various thicknesses, 2A12 aluminum plates named “bumper”, and 6.35-mm-diameter, 2017 aluminum spheres are presented and described. Impact velocities for these tests were between 2.23 km/s and 5.26 km/s. The morphological features such as components and shape, and the formation process of the debris clouds were discussed and compared with those presented by Piekutowski. As a result, the front element of debris cloud observed by Piekutowski was not evident in views of the debris clouds in this paper. A certain value of t/D ratio (bumper thickness to sphere diameter ratio), at two sides of which, the formation process of the internal structure of the debris cloud were different existed. The distance between the external bubble and the primary element decreased as the t/D increased regardless of impact velocity. The size and number of fragments in the debris clouds were not evaluated quantitatively, but described qualitatively.

1. INTRODUCTION

Hypervelocity impact between orbital debris, meteoroids and spacecraft can lead to significant damage and failure due to the high impact velocity[1,2]. The concept of using a single thin plate named “bumper” placed at a short distance ahead of a primary structural system or component as a means of mitigating hypervelocity impact damage was originally proposed by Whipple in 1947[1]. Spheres have been used as simulants of micrometeoroids and fragments of space debris for many hypervelocity impact tests performed during the past 50 years; they continue to be used as simulants for tests currently being performed[3].

The first thin plate (bumper) would disintegrate the orbital debris and meteoroids into debris cloud by the hypervelocity penetration. The features of debris cloud form the basis for evaluation of damage on rear walls. Excellent radiographs and systematic quantitative descriptions of debris clouds produced by both normal and oblique hypervelocity impact were presented by Piekutowski[3]. However, most of these tests using aluminum spheres and bumpers were performed with relatively lower t/D ratio (bumper thickness to sphere diameter ratio) and higher impact velocity. More radiographs of debris cloud for various impact

conditions will broaden the research scope of debris cloud. As we know, x-ray radiography can offer views into the structure and propagation of debris cloud[3]. The outline of fragments in debris cloud appear more clearly in radiographs than photographs taken by high speed camera which can be affected by impact flash and the black cloud produced by the impact of a sabot with the bumper[4].

In the present research, the radiographs of debris clouds in 20 hypervelocity impact tests are presented. All tests were performed using 6.35-mm-diameter, 2017 aluminum spheres as projectile, and 0.5-, 1.0-, 1.5-, 2.0-mm-thick, 2A12 aluminum plates as bumper. All debris clouds were only qualitatively described and discussed, and some phenomena and results similar or dissimilar to Piekutowski’s were found. More quantitative analysis of these debris clouds will be given in later papers.

2. EXPERIMENTAL SETUP

All hypervelocity impact tests were performed using a 57/10 mm, two-stage, light-gas gun in Hypervelocity Impact Research Center of HIT (Harbin Institute of Technology). The projectile was contained in a cylindrical plastic sabot consisting of two pieces. The sabot was separated from the projectile by the gas dynamic drag force in flight and as such was deflected from the path of the projectile, i.e. the ballistic line. Impact velocity determinations were made with use of a system which mainly consists of a magnetic induction part and a digital wave memory device. Accuracy of the impact velocity determination is about $\pm 1\%$.

Twenty tests were performed using 6.35-mm-diameter, 2017 aluminum spheres with velocity, v , ranging from 2.23 km/s to 5.26 km/s. Four thicknesses of 2A12 aluminum plates, 0.5-, 1.0-, 1.5-, and 2.0-mm, were used as bumpers. In addition, a 2A12 aluminum plate was placed 350 mm downrange of the bumper for each test as a witness plate to record the damage pattern produced by the impact of debris clouds. The detailed test conditions are shown in Tab. 1. All bumpers which were 100 mm square and witness plates which were 300 mm square were installed normal to the range center line.

Table 1. Test Condition

Test Number	Bumper Thickness t (mm)	Impact Velocity v (km/s)	Test Number	Bumper Thickness t (mm)	Impact Velocity v (km/s)
DT-01	0.5	2.31	DT-11	1.5	2.25
DT-02	0.5	2.98	DT-12	1.5	3.05
DT-03	0.5	3.49	DT-13	1.5	3.53
DT-04	0.5	4.24	DT-14	1.5	4.17
DT-05	0.5	5.00	DT-15	1.5	5.00
DT-06	1.0	2.27	DT-16	2.0	2.23
DT-07	1.0	3.02	DT-17	2.0	3.00
DT-08	1.0	3.23	DT-18	2.0	3.25
DT-09	1.0	3.78	DT-19	2.0	4.31
DT-10	1.0	4.25	DT-20	2.0	5.26

In 18 tests, a flash, soft x-ray radiography system (Scandiflash, Sweden, Model XT-150, pulse duration of 35 ns) consisting of four pairs of x-ray heads was used to provide simultaneous, orthogonal views of debris cloud. The exposure area of each x-ray beam was appropriately arranged on the x-ray films by using x-ray shields outside of the chamber. Two sheets of x-ray film were set in the film cassettes below the target consisting of bumper and witness plate. The ratio of the x-ray-source-to-ballistic-line to ballistic-line-to-x-ray-film distance was 6:1. The x-ray emission time of each source was controlled with a delay pulse unit. The test setup is shown in Fig. 2. The first pair of x-ray heads was used to view and record the position of the bumper and the debris clouds a few microseconds after impact. Other pairs of x-ray heads were used to produce views of the debris clouds at three positions along ballistic line.

Due to the large axial size of the debris clouds, in test DT-15 and DT-20, only two pairs of x-ray heads were working and one pair of x-ray shields was kept in use as shown in Fig. 1.

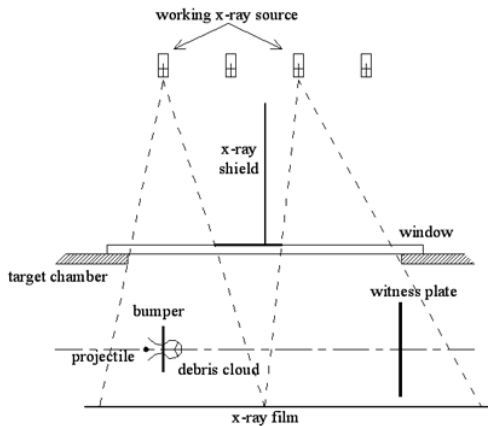
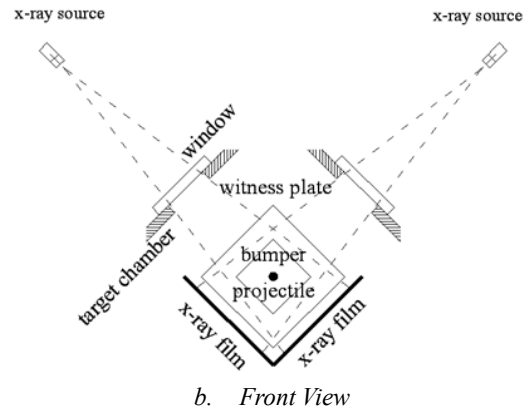
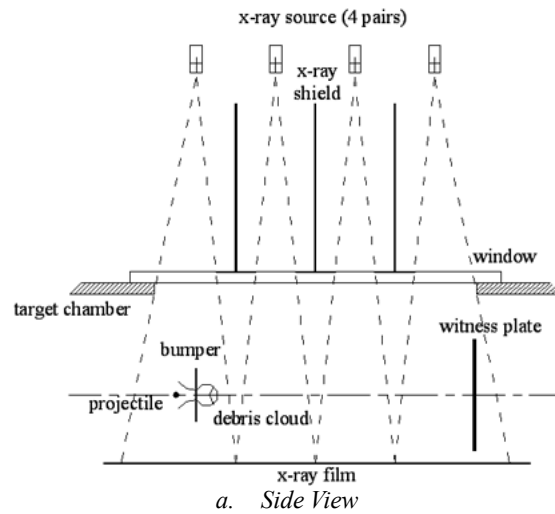


Figure 2. Setup Used to Obtain Orthogonal-Pair Radiographs of Debris Clouds

Figure 1. Setup Used for Test DT-15 and DT-20

3. DESCRIPTION OF DEBRIS CLOUDS

Since two radiographs of the debris clouds simultaneously taken by the x-ray tubes positioned orthogonally were similar, Fig. 3 ~ Fig. 22 give radiographs produced by x-ray tubes at one side of the chamber for all tests. According to the test setup, two pairs of radiographs shown in Fig. 17 and Fig. 22 were produced in test DT-15 and DT-20, while other tests should present four pairs of radiographs of debris cloud. However, in test DT-10 and DT-17, only three radiographs shown in Fig. 12 and Fig. 19 were seen due to mistakes in calculation of x-ray emission time. In this paper, all radiographs are shown with the same scale.

Several nomenclatures of the elements of debris cloud given by Piekutowski in [3] will be used in this portion, such as ejecta veil, external bubble, spall shell, and large central fragment.

3.1. Debris Clouds in Tests with Bumper Thickness of 0.5 mm

Debris clouds after impacts with bumper thickness of 0.5 mm and various impact velocities are shown in Fig. 3 ~ Fig. 7. In test DT-01, plastic deformation of the front (impacting) surface of the sphere without fragmentation was evident. In test DT-02, the spall shell on the rear of the sphere ruptured and formed petals that remained attached to the deformed sphere. In test DT-03, fragmentation of the spall shell separated from the more heavily deformed sphere occurred. In test DT-04, besides the further development of the spall shell, materials on the periphery of the main body of the sphere broke up and go away from a large central fragment. In test DT-05, fragmentation of the large central fragment occurred.

The following observations are common for these five tests: (1) the ejecta veil consisting of bumper debris with too little size was difficult to be seen from the radiographs, (2) the external bubble of debris absolutely embraced the debris cloud composed of sphere material without interaction.

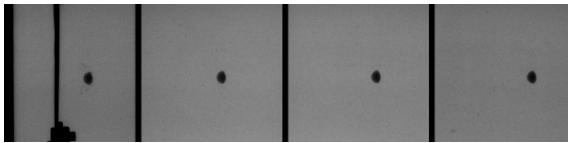


Figure 3. Radiographs of Debris Cloud in Test DT-01

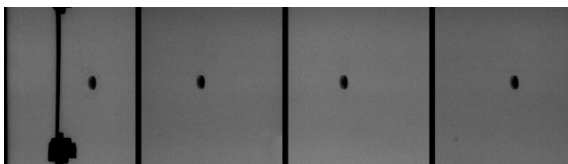


Figure 4. Radiographs of Debris Cloud in Test DT-02

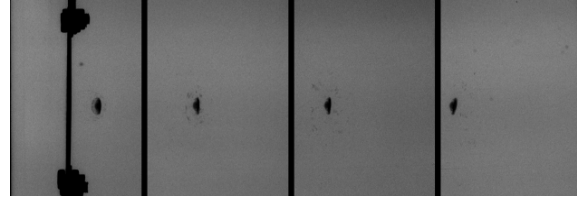


Figure 5. Radiographs of Debris Cloud in Test DT-03

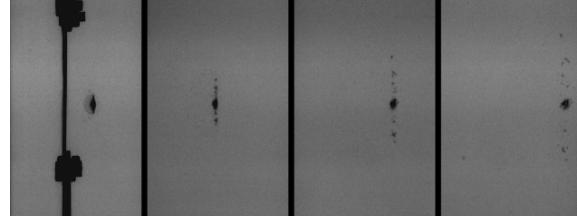


Figure 6. Radiographs of Debris Cloud in Test DT-04

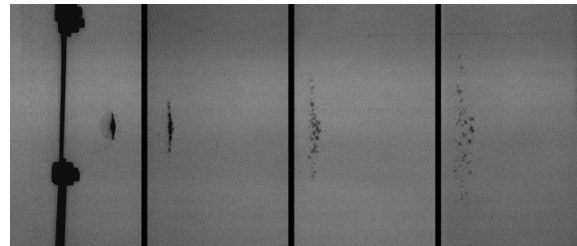


Figure 7. Radiographs of Debris Cloud in Test DT-05

3.2. Debris Clouds in Tests with Bumper Thickness of 1.0 mm

Debris clouds after impacts with bumper thickness of 1.0 mm and various impact velocities are shown in Fig. 8 ~ Fig. 12. In test DT-06, larger plastic deformation of the sphere without fragmentation than that in test DT-01 was evident. In test DT-07, fragmentation of the spall shell separated from the more heavily deformed sphere occurred. In test DT-08 ~ DT-10, fragmentation of the spall shell and the main body of sphere occurred, and the size of fragments in these two elements decreased as impact velocity increased.

For the debris clouds in these five tests, the front portion of the external bubble almost located at the same position with the front surface of the debris cloud composed of sphere material. Very faint ejecta veils were formed, but were difficult to reproduce for presentation in the figures.

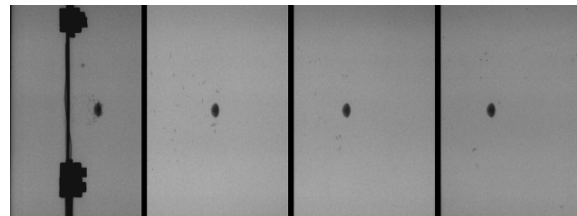


Figure 8. Radiographs of Debris Cloud in Test DT-06

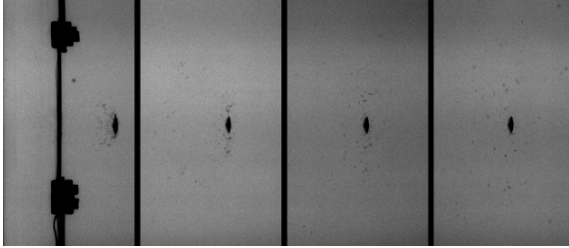


Figure 9. Radiographs of Debris Cloud in Test DT-07

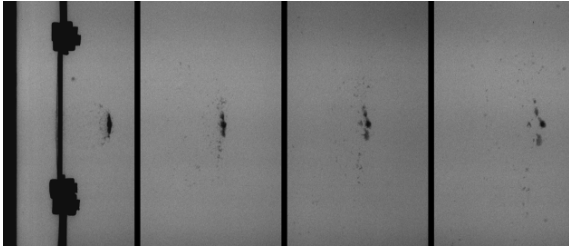


Figure 10. Radiographs of Debris Cloud in Test DT-08

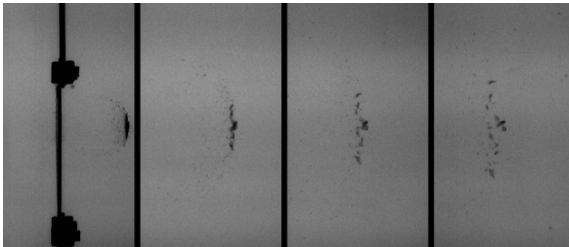


Figure 11. Radiographs of Debris Cloud in Test DT-09

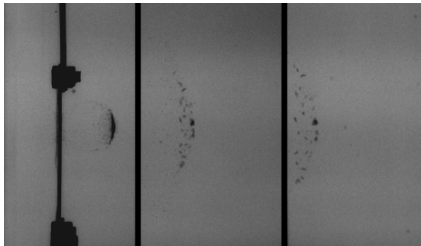


Figure 12. Radiographs of Debris Cloud in Test DT-10

3.3. Debris Clouds in Tests with Bumper Thickness of 1.5 mm

Debris clouds after impacts with bumper thickness of 1.5 mm and various impact velocities are shown in Fig. 13 ~ Fig. 17. In test DT-11, large plastic deformation was represented by the front surface of sphere bending over backwards and the rear surface flattened a little after compression. In test DT-12, fragmentation of the main body of sphere occurred without a spall shell. In test DT-13 and DT-14, the spall shell appeared behind the primary element of the debris cloud consisting of materials of the sphere's main body. In test DT-15, a piece of sabot impacting on the bumper and traveling with the debris cloud was observed. The front surface of the primary element was like a bowl.

In the five radiographs shown in Fig. 13 ~ Fig. 17, the ejecta veils were displayed since the fragments spraying from the relative thick bumper were relative large. The front surface of the external bubble overtaken by fragments in the primary element was no found.

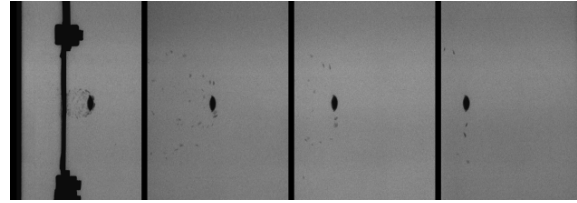


Figure 13. Radiographs of Debris Cloud in Test DT-11

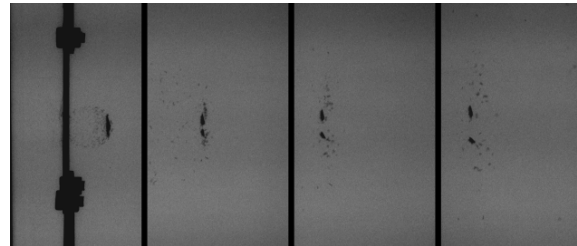


Figure 14. Radiographs of Debris Cloud in Test DT-12

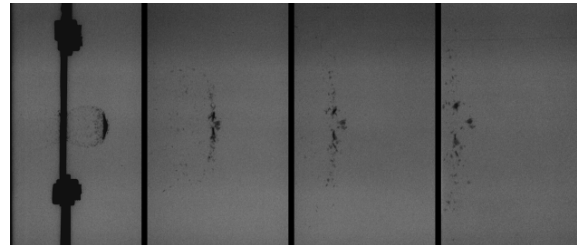


Figure 15. Radiographs of Debris Cloud in Test DT-13

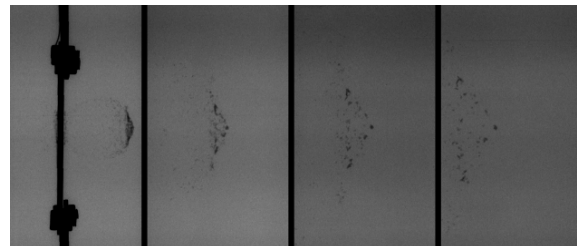


Figure 16. Radiographs of Debris Cloud in Test DT-14

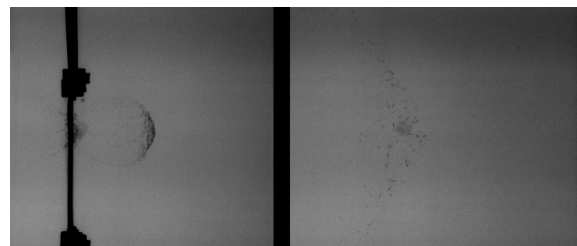


Figure 17. Radiographs of Debris Cloud in Test DT-15

3.4. Debris Clouds in Tests with Bumper Thickness of 2.0 mm

Debris clouds after impacts with bumper thickness of 2.0 mm and various impact velocities are shown in Fig. 18 ~ Fig. 22. In test DT-16, the materials in the periphery of the disk-like projectile were extruded backwards with a nearly flat rear surface. In test DT-17 and DT-18, fragmentation of the main body of sphere occurred without a spall shell. No one outstanding large central fragment was found. In test DT-19 and DT-20, the spall shell appeared again. The shape of the front surface of the primary element changed from an umbrella to a bowl.

In the five radiographs shown in Fig. 18 ~ Fig. 22, the ejecta veils could be distinctly observed. The front portion of the external bubble overtaken by fragments in the primary element was not seen. The views of test DT-19 and DT-20 that are presented in Fig. 21 and Fig. 22, clearly showed a fairly large and continuous overturned flap on both sides of the bumper.

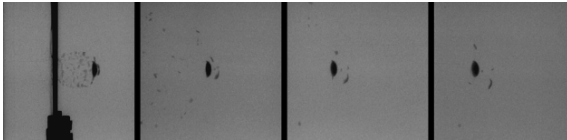


Figure 18. Radiographs of Debris Cloud in Test DT-16

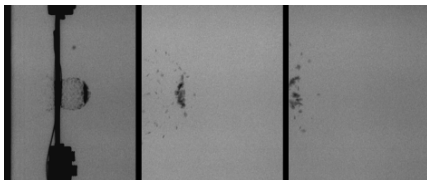


Figure 19. Radiographs of Debris Cloud in Test DT-17

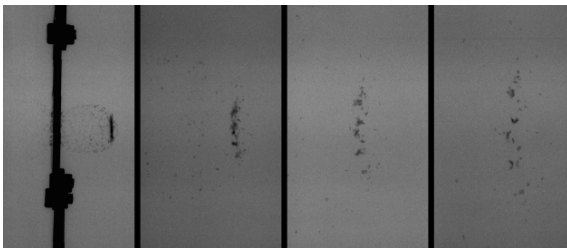


Figure 20. Radiographs of Debris Cloud in Test DT-18

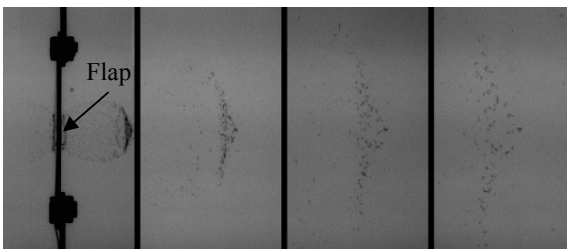


Figure 21. Radiographs of Debris Cloud in Test DT-19

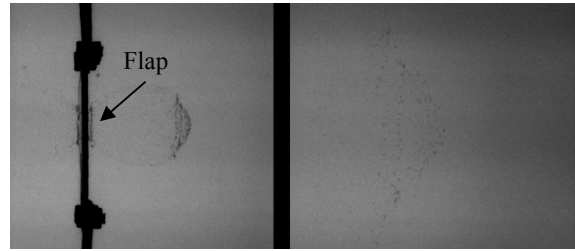


Figure 22. Radiographs of Debris Cloud in Test DT-20

4. DISCUSSION

4.1. Major Debris-Cloud Features and Elements

Typical illustration of the major features of debris cloud were presented by Piekutowski[3]. First, an ejecta veil, consisting almost entirely of bumper fragments, was ejected from the impact or front side of the bumper. Second, an expanding external bubble of bumper debris formed on the rear side of the bumper. Finally, an internal structure composed of projectile debris located inside and at the front of the external bubble. The internal structure was composed of a front, center, and rear element (spall shell).

A view of a debris cloud is presented in Fig. 23 to illustrate the major features of the debris cloud. All features but the front element mentioned above were evident in the views of the debris clouds in this paper likely due to lower impact velocities than those of Piekutowski's tests. The internal structure, i.e. the debris cloud composed of projectile debris, consisted of two parts: spall shell and primary element. Definitions of the ejecta veil and the external bubble in [3] were available for the debris clouds in this study.

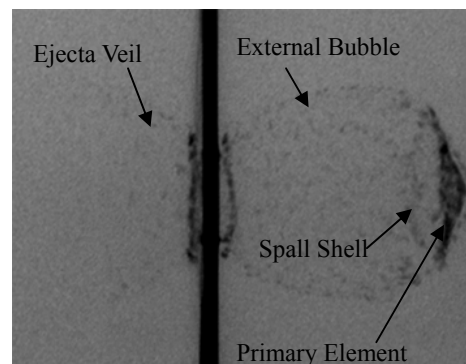


Figure 23. Morphological Features and Elements of a Debris Cloud Produced in Test DT-19

4.2. Characteristics of Spall Shell and Primary Element

Formation of the internal structure initiated by hypervelocity impact was two kinds of orderly processes for various bumper thicknesses, t . Several stages of the internal structure formation for tests with

bumper thicknesses of 0.5 and 1.0 mm as impact velocity was varied are shown in Fig. 3 ~ Fig. 12. When impact velocities were low, plastic deformation of the sphere occurred. At higher impact velocities, a shell of spall fragments developed when the spall layer broke open and the spall petals separated from the back of the sphere. As impact velocity continued to increase, a cloud of sphere fragments formed and eventually developed into a structure with the two elements (the ejecta veil and the primary element). As shown in Fig. 13 ~ Fig. 22, for tests with bumper thickness of 1.5 and 2.0 mm, the sphere broke up without spall shell when impact velocity was increased above that required to produce plastic deformation of the sphere. As impact velocity increased, spall shell appeared in the whole internal structure of the debris cloud. It permits an assumption that there should be a threshold value of bumper thickness, t_{sp} . When $t > t_{sp}$, the visible spall shell comes into being after materials in the primary element break up. If only $t < t_{sp}$, the view of a spall shell with a deformed sphere observed by Piekutowski can be seen.

Several qualitative results for tests with same bumper thickness were gained: (1) the number of fragments in the primary element increased and the size of those fragments decreased as the impact velocity increased; (2) the axial size of the primary element increased with the increasing impact velocity.

4.3. Characteristics of Ejecta Veil and External Bubble

The distance between the external bubble and the primary element decreased as the bumper thickness increased regardless of impact velocity. For tests with bumper thickness of 0.5 mm, the external bubble of debris absolutely embraced the internal structure without interaction. For tests with bumper thickness of 1.0 mm, the primary element almost attached the front portion of the external structure. For tests with 1.5 and 2.0 mm, the front portion of the external structure overtaken by the primary element was not distinguished in views of the debris clouds.

A large and continuous overturned flap on both sides of the bumper introduced by Piekutowski only came into being for a combination of relative large impact velocity and bumper thickness.

Sizes of fragments in the ejecta veil and the external bubble spayed from thick bumper were larger than those from thin bumper.

5. SUMMARY AND CONCLUSIONS

Debris clouds produced by 20 hypervelocity impacts

performed for a degree thesis were presented and described. Although spheres with a same diameter of 6.35 mm were used in these tests, conclusions on the morphological features of the debris clouds drawn from previous analysis are available for all impacts with the similar t/D ratio and impact velocity[6]. The morphological features of the debris clouds presented by Piekutowski[3,5] were observed in this research, except for the front element. There should be a threshold value of bumper thickness to sphere diameter ratio, $(t/D)_{sp}$. When t/D was larger or less than $(t/D)_{sp}$, the orders of appearances, for the first time, of the spall shell and primary element breaking up were different. The distance between the external bubble and the primary element decreased as the t/D increased regardless of impact velocity.

An obvious phenomenon was observed in the radiographs that sizes of fragments in the debris clouds back of bumper decreased as impact velocity increased when sphere diameter and bumper thickness kept constant.

All conclusions given above are qualitative, and further quantitative analysis and discussions of these debris clouds, including the velocities of the debris clouds and the damage patterns of the witness plates, will be performed in later papers.

6. REFERENCES

1. Bernhard, P.P., Christiansen, E.L., Hyde, J., & Crews, J.L. (1995). Hypervelocity Impact Damage into Space Shuttle Surfaces. *Int. J. Impact Engng.* **17**(1-3), 57-68.
2. Christiansen, E.L. (1995). Enhanced Meteoroid and Orbital Debris Shielding. *Int. J. Impact Engng.* **17**(1-3), 217-228.
3. Piekutowski, A.J. (1996). Formation and Description of Debris Cloud Produced by Hypervelocity Impact. CR-4707.
4. Chi, R.Q., Pang, B.J., Guan, G.S., Yang, Z.Q., Zhu, Y., & He, M.J. (2008). Analysis of Debris Clouds Produced by Impact of Aluminum Spheres with Aluminum Sheets. *Int. J. Impact Engng.* **35**(12), 1465-1472.
5. Piekutowski, A.J. (1995). Radiographic Studies of Impact Fragmentation. In *High-Pressure Shock Compression of Solids II* (Eds. Davison), Springer-Verlag, New York, USA, pp 150-175.
6. Piekutowski, A.J. (1997). Effects of Scale on Debris Cloud Properties. *Int. J. Impact Engng.* **20**(6-10), 639-650.